

Experimental Observation of Projectile Deflection in the Fields of Rotating Spheres

J.F. Cuderman

**Retired Distinguished Member of the Technical Staff, Sandia National Laboratories*

jfcuderman@gmail.com

(Dated 8/7/20)

Abstract

Experiments were performed to measure the deflection of projectiles moving past rotating spheres. A theory of an inertial gravitational Co-Field, proposed by the author, predicted such deflections. Deep space mission spacecraft flybys of the earth revealed anomalous deflections of spacecraft. The present experiments explore such deflections as a function of experiment geometry, projectile velocity, sphere angular velocity, and solid or hollow spheres. The Co-Field theory correctly predicted projectile deflections. It explained several unanticipated data results and revealed the need for a Co-Field Constant Multiplier to the model.

I. INTRODUCTION

The proposed gravitational Co-Field theory together with the spacecraft flyby anomalies prompted this experimental study. Upon completion of the Co-Field theory, it was unclear whether any corroborating data existed [1]. A literature survey revealed the Anderson et.al. paper [2] on spacecraft-earth flyby anomalies. Anomalous changes in velocity were measured during spacecraft-Earth flybys on deep space missions launched between 1990 and 2006. A semi-empirical description which is in agreement with results for the anomalous velocity deflections was developed by Anderson et al. Numerous attempts to explain the data were unsuccessful [3]. It was seen that the Co-Field theory provided a physical basis for the semi-empirical model and the observed deflections. The present experimental study further explores the interaction of objects moving in the field of rotating spheres.

A theorem by Helmholtz [4] states that a complete field is defined by the combination of an irrotational, conservative field and a rotational, solenoidal field. Coulombs Law which defines the electric field and the magnetic field are such fields. The fundamental basis of the Gravity and Co-Field model is that the total force acting on a mass moving in a gravitational Co-Field is given by Newton's law of universal gravitation field plus a rotational Co-Field. The generalized total field, $\Gamma = F/m$, used to develop the field equations of gravitation, is

$$\Gamma = \frac{F_g}{m} = \frac{M}{4\pi\epsilon_{og}r^2}\hat{r} + r\ddot{\theta}\hat{\theta} \quad (1)$$

with the gravitational constant G , replaced by $G = 1/4\pi\epsilon_{og}$. The electromagnetic equivalent of Equation (1) is

$$E = \frac{Q}{4\pi\epsilon_or^2}\hat{r} + \frac{m}{q}r\ddot{\theta}\hat{\theta} \quad (2)$$

Because the two equations are so similar, operations on either will yield functionally similar results. Maxwell's equations, as reduced to four vector equations by Heaviside [5], were deduced from the experimental data of that time. The same divergence and curl operators used on Equation (2) also produce Maxwell's equations. The Co-Field model generally uses the curl in differential form, expressed in cylindrical coordinates. This approach defined the Co-Field Ω , the acceleration of a mass having a velocity V in the Co-Field, and an Ω dipole.

II. GRAVITATIONAL CO-FIELD MODEL

Section II is a brief summary of the gravitational Co-Field model. It shows the derivation of results listed above. Results are also presented for the parallel analysis in electromagnetism.

A. Inertial and Electrical Co-Fields

The fundamental assumption of the Gravity and Co-Field model is that the total force acting on a mass moving in a gravitational Co-Field is given by Newton's inverse square force plus a rotational force. The generalized total field, $\Gamma = \mathbf{F}/m$, used to develop the field equations of gravitation, with the traditional gravitational constant, G , replaced by $G = 1/4\pi\epsilon_{og}$ is

$$\Gamma = \frac{F_g}{m} = \frac{M}{4\pi\epsilon_{og}r^2}\hat{r} + r\ddot{\theta}\hat{\theta} \quad (1)$$

This re-definition of G in Equation (1) is done to put the gravitational equation into the same format as for electrical force and to develop the gravitational equivalents of permeability and permittivity for the co-field dipole field. The electromagnetic analog of Equation (1) is

$$\mathbf{E} = \frac{Q}{4\pi\epsilon_0r^2}\hat{r} + \frac{m}{q}r\ddot{\theta}\hat{\theta} \quad (2)$$

The divergence and curl of Equation (2) and of its resulting co-field \mathbf{B} results in Maxwell's equations. In Equation (2), the first term is irrotational and therefore the curl is zero; the second, rotational term is non-zero. Conversely, the divergence of the first term is non-zero and the second term is zero. With $\nabla \times \mathbf{V}$ expressed in cylindrical coordinates and considering the z component only, the differential form of the curl of Equation (1) results in:

$$\nabla \times \Gamma = \frac{\partial}{\partial t} (2\dot{\theta})\hat{z} = \frac{\partial \Omega}{\partial t} \quad (3)$$

$$\Omega = 2\omega \quad (4)$$

In E&M, \mathbf{B} has the units of M/QT so $\nabla \times \mathbf{E}$ yields

$$\mathbf{B} = \frac{m}{q}\omega \quad (5)$$

Thus, both the \mathbf{B} field and the inertial Ω field are angular velocity fields with the difference that the \mathbf{B} field carries mass and charge.

B. The Dimensional Constants ϵ_0 and μ_0 ; ϵ_{og} and μ_{og}

In the case of Electromagnetism, ϵ_0 is a universal constant, but only because a single particle is involved, the electron. Starting with Coulomb's law and invoking dimensional analysis,

$$F = \frac{q^2}{4\pi\epsilon_0R^2} \quad (6)$$

$$M\frac{L}{T^2} = \frac{Q^2}{4\pi\epsilon_0L^2} \quad (7)$$

$$\epsilon_0 = \frac{Q^2 T^2}{4\pi ML L^2} \quad (8)$$

Noting that Equation (8) has the familiar form of $\epsilon_0 = 1/\mu_0c^2$

$$\epsilon_0 = \left[\frac{q^2}{4\pi mr_0} \right] \left[\frac{T^2}{R^2} \right] = \frac{1}{\mu_0c^2} \quad (9)$$

$$\mu_0 = \frac{4\pi mr_0}{q^2} \quad (10)$$

Let r_0 equal the Thompson electron radius, M the electron mass, and q its charge. Re-arranging and setting $r_0/t = c$, the speed of light, yields $\mu_0 = 4\pi \times 10^{-7}$. Since both μ_0 and c are constants, ϵ_0 is a constant.

The derivation of μ_0 and its value provides a basis for a similar approach to determining its gravitational counterpart μ_{0g} . For the gravitational case, a possible constant K was introduced as part of the dimensional analysis. It was seen in the Gravitational & Co-Field theory [1] that K=2.

$$\frac{F}{m} = \frac{M}{K4\pi\epsilon_{0g}L^2} = \frac{L}{T^2} \quad (11)$$

Re-arranging and assigning $L=R_0$ one has, dimensionally

$$\epsilon_{0g} = \frac{M}{8\pi R_0} \left[\frac{T^2}{R^2} \right] = \frac{1}{\mu_{0g}v^2} \quad (12)$$

$$\mu_{0g} = \left[\frac{8\pi R_0}{M} \right] \quad (13)$$

As is the case for μ_0 , μ_{0g} is also a constant but is a constant for only the principal R_0 and M of a given system. To illustrate, for the Earth-Moon system R_0 is the Earth's radius and M is its mass. For the Sun and its planets, R_0 is the radius of the sun and M its mass.

That ϵ_{0g} and G are constants is shown by re-formatting Equation (11) with its dimensional terms

$$\frac{1}{K4\pi\epsilon_{0g}} = G = \frac{1}{M} \frac{L^3}{T^2} = \frac{K' R^3}{M T^2} \quad (14)$$

The final term in Equation (14) is recognized as Euler's 3rd Law which is a constant. The constant K' determines the system of units employed. This is a variation of the standard derivation of Kepler's 3rd law.

C. The Inertial Dipole Field

The following relationship was determined using the differential form of the curl:

$$\nabla \times \mathbf{\Omega} = (\mu_{0g} \mathbf{J}_m + \frac{1}{v^2} \frac{\partial \Gamma}{\partial t}) \hat{\mathbf{z}} \quad (15)$$

The first term of Equation (15) is the basis for an inertial version of the Biot-Savart equation for magnetism:

$$d\Omega = \frac{\mu_{0g} i dl \sin\theta}{4\pi R^2} \quad (16)$$

Assuming a mass in a circular orbit, whose current is M/T, and integrating to obtain the value of Ω along the axis yields

$$\Omega = \frac{\mu_{0g} i R^2}{2 (R^2 + Z^2)^{3/2}} \quad (17)$$

where R is the distance from a point on the circular orbit to a point on the axis and Z is the distance from the center of the orbit to a point on the axis. If $R=0$, the value of Ω at the orbit center is 2ω . Multiplying both numerator and denominator of Equation (17) by π and setting $R=0$ yields, with $iA = i\pi R^2 = \mu_g$,

$$\Omega = \frac{\mu_{0g} \mu_g}{2\pi Z^3} \quad (18)$$

The radial value, from the axis, $Z=0$, for a dipole in the equatorial plane is 1/2 the axial value.

$$\Omega = \frac{\mu_{0g} \mu_g}{4\pi R^3} \quad (19)$$

In Equation (3), $\nabla \times \mathbf{\Omega}$ defined the inertial co-field Ω . The integral form of curl Γ is derived from

$$a_\theta (2\pi r) = \frac{d}{dt} (2\omega \pi r^2) \quad (20)$$

Assuming an acceleration in a circular orbit, of radius r and area A , normal to the Ω field of 2ω .

$$\mathbf{a}_\theta = (2\omega \dot{\mathbf{r}} + \dot{\omega} \mathbf{r}) \quad (21)$$

Since both ω and $\dot{\omega}$ are both normal to \mathbf{r} and $\dot{\mathbf{r}}$ Equation (21) stated in vector form, is

$$\mathbf{a}_\theta = 2\omega \times \dot{\mathbf{r}} + \dot{\omega} \times \mathbf{r} \quad (22)$$

The first term on the right in Equation (22) is interpreted as the acceleration of an object moving with velocity $\mathbf{V} = \dot{\mathbf{r}}$ in an angular velocity field $\Omega = 2\omega$. The second term is the acceleration due to a time dependent angular velocity. Both terms in Equation (22) also appear in classical solid mechanics for the acceleration of an object moving in a rotating frame. The first term in the equation is recognized as the Coriolis acceleration. Both terms of Equation (22) are designated as "fictitious" accelerations in classical mechanics. They are, in the Co-Field formulation, terms of inertial induction. The first term on the right in Equation (22) is the inertial equivalent of the $\mathbf{V} \times \mathbf{B}$ acceleration in E &M, and ω is constant in the present application. Thus, the second term is zero.

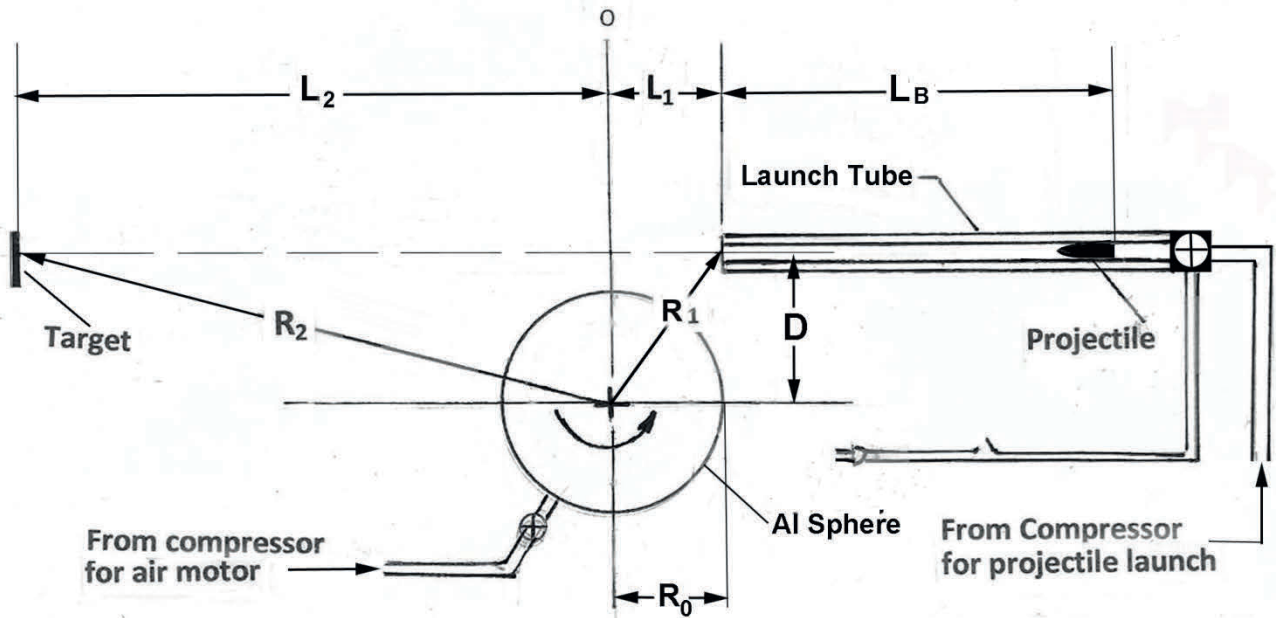
$$\mathbf{a}_\theta = 2\omega \times \mathbf{V} = \Omega \times \mathbf{V} \quad (23)$$

III. EXPERIMENT DESCRIPTION AND PROJECTILE VELOCITIES

A. Experiment Description

Experiments were conducted to measure the predicted deflection of a projectile due to the inertial dipole field of rotating spheres. Figure 1 is a schematic of the experiment setup. The experiment used 50.8 mm nominal diameter aluminum spheres spinning at 1676 radians/s. One 50.8 mm sphere was of solid aluminum. A second 50.8 mm diameter sphere was hollow with a 3.2 mm wall thickness. The sphere/airmotor assembly mounted on a stand independent of the projectile barrel-target platform. A cardboard shield isolated the flight path of the projectile from aerodynamic effects of the spinning sphere. The sphere equator was in the same plane as the projectile barrel centerline. The distance between the sphere and airmotor rotor centers was about 130 mm.

From the flyby semi-empirical model [2] and the Gravitational & Co-Field theory [1] a spinning sphere should produce an inertial dipole field normal to the diametric plane of the sphere. The field at its center should be equal to twice the angular velocity ω of the spheres and decrease as the inverse cube of the distance from the origin. A compressor driven, reversible, airmotor spun the spheres to 1676 radians/s. The airmotor switch opened the air to the airmotor from a compressor tank charged to 0.862 MPa. Experiment dimensions are listed in Figure 1. A thick walled, nominal 3.2 mm ID stainless steel tube served as a launch tube. The launch tube center line was coincident with the equatorial plane of the rotating sphere. A 3.175 mm diameter, 23 mm long, pointed, tool steel projectile was launched using a second compressor. Projectiles of aluminum and brass were used in initial tests, but tips deformed after a few shots. The steel projectiles did not deform, and no magnetic effects were observed. Deflections were essentially the same as for brass. Launch of the projectile was initiated by a momentary electrical switch which opened a solenoid valve. Projectile launch pressures of 276 and 724 kPa were used in initial tests. The launch barrel length was 70 cm. The flight path from barrel exit to a plastic target was 95 cm. The vertical drop due to gravity, from the barrel exit to the target, provided the data for determining the projectile velocity. As in all ballistic tests there was a spread in impact points at the target. Thus, at least 10 shots were conducted at each launch pressure both for dynamic tests where the sphere was rotating and static tests where it was not. Vertical inertial field displacements of projectiles, compared to gravitational, were minimal and are therefore neglected.



SPHERE OFFSET D	R ₀	L ₁	L ₂	L ₁ +L ₂	L _p	L _B
0.038 m	0.025	0.067	0.883	0.95	0.023	0.723
0.070 m	0.025	0.067	0.883	0.95	0.023	0.723

All dimensions above in meters; L_p = Projectile length

Figure 1. Experiment Schematic For Testing Projectile Deflection by Rotating Spheres

B. Projectile Velocity Calculated from Launch Pressure-Energy Gain

The simplest estimate of projectile velocity is to equate the energy gained in the acceleration barrel to the kinetic energy on exit.

$$PAL_B = \frac{1}{2}mV^2 \quad (24)$$

where P is the projectile driving pressure of 276 kPa or 724 kPa, A is the cross-sectional area of the launch barrel interior and L_B is the acceleration length in the barrel. The tool steel projectile mass is m, and V is the projectile velocity. The calculated barrel exit velocities are

$$V = 46.5 \text{ m/s for } P=276 \text{ kPa} \quad (25)$$

and

$$V = 75.7 \text{ m/s for } P=724 \text{ kPa} \quad (26)$$

It is noted that these results for velocities do not include any losses during the projectile launch and therefore represent an upper bound.

C. Velocity Calculated from Projectile Impacts

The results of this section establish the values for the velocities of projectiles launched with barrel pressures of 276 and 724 kPa, respectively. The resulting velocities were 40 m/s and 65 m/s, respectively. These velocities and quantities associated with them, will be designated by their velocity subscripts. For example, the velocity of a projectile launched with a barrel pressure of 276 kPa will be labeled V₄₀, that for 724 kPa, V₆₅. Similarly, coordinates associated with a given velocity will have the same subscript. The subsequent analysis derives the projectile velocities from the vertical displacements of projectile impacts on the target tiles.

If gravity were not acting on a projectile after leaving the launch barrel, the vertical impact point, Y_{0c}, on the target would be same regardless of velocity—a straight, horizontal path from the barrel exit. With gravity, faster

projectiles impact below Y_{0c} but higher than slower ones. Without sphere and airmotor rotation for the two projectile velocities V_{40} and V_{65}

$$Y_{40} + \Delta Y_{40} = Y_{0c} \quad (27)$$

$$Y_{65} + \Delta Y_{65} = Y_{0c} \quad (28)$$

Where Y_{40} and Y_{65} are measured values of projectile impacts as shown in Fig.2 in Section IV. ΔY_{40} and ΔY_{65} are the difference between the measured and no gravity value Y_{0c} . The displacement due to gravity from the barrel exit to the target is

$$\Delta Y = 1/2gt^2 \quad (29)$$

Where g is the gravitational acceleration 9.8 m/s^2 , $t=L/V$ is the time of flight, the flight path length is $L=L_1+L_2$, and V is the projectile velocity, assumed constant from barrel exit. Equation (29) reduces to

$$\Delta Y = \frac{4.42}{V^2} \quad (30)$$

$$\frac{\Delta Y_{65}}{\Delta Y_{40}} = \left[\frac{V_{40}}{V_{65}} \right]^2 \quad (31)$$

Projectile velocity at barrel exit assuming losses are constant over the experiment range of drive pressures is

$$\lambda P A L_B = \frac{1}{2} m V^2 \quad (32)$$

Then

$$\frac{P_{40}}{P_{65}} = \left[\frac{V_{40}}{V_{65}} \right]^2 = \frac{276}{724} = 0.381 \quad (33)$$

$$\Delta Y_{65} = 0.381 \Delta Y_{40} \quad (34)$$

From Equations (27) and (28)

$$Y_{40} + \Delta Y_{40} = Y_{65} + \Delta Y_{65} \quad (35)$$

Substituting ΔY_{65} from Equation (34) yields

$$\Delta Y_{40} = 1.62(Y_{65} - Y_{40}) \quad (36)$$

Averages for Y_{65} and Y_{40} were $Y_{65} = 23.68 \times 10^{-3} \text{ m}$ and $Y_{40} = 21.96 \times 10^{-3} \text{ m}$ resulting in $\Delta Y_{40} = 2.79 \times 10^{-3} \text{ m}$, and $\Delta Y_{65} = 1.06 \times 10^{-3} \text{ m}$. $Y_{0c} = 24.75 \times 10^{-3} \text{ m}$.

Final values for the projectile velocities based on tile impact data are:

$$V_{40} = 40 \text{ m/s} \quad (37)$$

$$V_{65} = 65 \text{ m/s} \quad (38)$$

IV. DATA AND DATA ANALYSIS

A. Data Measurements

Each test started with a fresh plastic target tile. Pressures were adjusted for both the airmotor and the projectile launch compressors. The compressor powering the airmotor was set to 0.862 MPa to produce 1676 radian/s rotation. The projectile launch compressor was set to either 276 or 724 kPa, yielding projectile velocities of 40 or 65 m/s, respectively. Due to the spread in impact points at the target, at least 10 projectile launches were conducted for a given pressure, both for dynamic and static tests as noted earlier. Each experiment yielded lateral displacements L_0 , L_R , L_L , and vertical displacements: Y_0 , Y_R , Y_L . The subscripts 0, R, and L refer, respectively, to No, Right (CCW), and Left (CW) rotations, of the sphere. Figure 2 is a schematic of a target identifying the measured data. Table 1 presents L_0 , L_R , and L_L deflections of projectiles moving past an aluminum sphere in its equatorial plane. The L values were measured from the projectile impacts as indicated in Figure 2.

The L_0 projectile deflections are for no sphere and airmotor rotation. L_R is the projectile deflection resulting from right hand rotation (CCW) of the sphere as viewed from above. L_L is the corresponding left-hand rotation induced deflection. The projectile impact deflections were measured with a digital caliper. Each entry in the table represents the average of 10 data points.

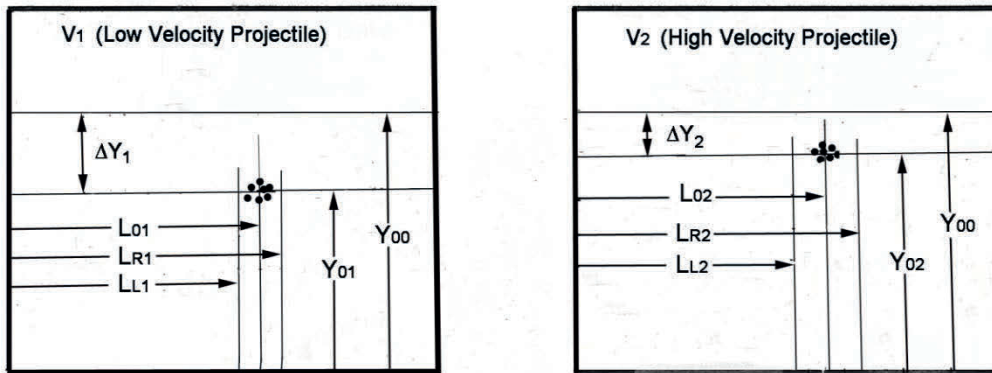


Figure 2. Target Tile Schematic Showing Measured Data

B. Total Deflection Measurements

In Table 1, ΔL_R and ΔL_L are the respective difference values from L_0 . The values of ΔL_R should be positive and those of ΔL_L negative. This is required by the right and left respective sphere rotations. It is seen that the most prominent deflection data are for ΔL_R for solid spheres, with 40 m/s projectile velocities. It was recognized that the measured total deflections are due not only to the inertial field produced by the spinning sphere, but a combination of the deflections of the sphere and the airmotor rotor dipole fields. The total deflections are measurements from the combined fields. To determine the sphere-only contribution, it is necessary to measure the deflection produced by the airmotor alone. Assuming a simple superposition of fields, the difference between the ΔL_R and ΔL_L values of Table 1 and corresponding values of the rotating airmotor alone should yield the deflections due to the field of the rotating sphere. The ΔL values for the hollow spheres were smaller than the solid sphere values, as predicted by the Co-Field theory. Because of the larger deflections, subsequent data will be for solid spheres only.

Sphere Location*	Sphere Type	Projectile Velocity	Raw Data mm			$L_R - L_0$	$L_L - L_0$
			L_0	L_R	L_L		
D m	Al	V_P m/s	L_0	L_R	L_L	ΔL_R	ΔL_L
0.038	Hollow	40	29.89	28.53	29.82	-1.36	-0.07
0.038	Hollow	65	30.38	30.35	29.64	-0.03	-0.74
0.038	Solid	40	28.73	30.84	28.21	2.11	-0.52
0.038	Solid	65	28.32	30.75	29.37	2.43	1.05
0.070	Hollow	40	29.85	30.1	30.25	0.25	0.4
0.070	Hollow	65	29.64	30.37	30.11	0.73	0.47
0.070	Solid	40	27.67	30.25	28.32	2.58	0.65
0.070	Solid	65	30.56	29.83	30.39	-0.73	-0.17

Table 1. "L" Deflections as a Function of 50.8 mm Sphere Location, Geometry and Projectile Velocity

C. Separation of Sphere and Airmotor Dipole Field Deflections

Measurements of L_0 , L_R , and L_L , with the sphere removed, provided the data for the airmotor-only deflections. Figure 1 identifies the 38 and 70 mm sphere offset locations D. Table 2 provides results from the D-38 mm location; Table 3 from the 70 mm location. Results Include Total, airmotor-only, and sphere-only induced deflections for solid 50.8 mm diameter spheres for 40 and 65 m/s projectile velocities.

SOLID SPHERE DEFLECTIONS		
D=38mm Location	Deflections (mm)	
Deflections: V = 40m/s	ΔL_R	ΔL_L
Total	2.11	-0.52
Air Motor	1.04	1.8
Sphere	1.07	-2.32
Deflections: V = 65 m/s	ΔL_R	ΔL_L
Total	2.43	1.05
Air Motor	1.89	1.42
Sphere	0.54	-0.37

Table 2. AI Sphere Data Showing Total, Airmotor (No Sphere), and Sphere Deflections (D=38 mm)

SOLID SPHERE DEFLECTIONS		
D=70mm Location	Deflections (mm)	
Deflections: V = 40m/s	ΔL_R	ΔL_L
Total	2.58	0.65
Air Motor	0.58	0.85
Sphere	2.00	-0.20

Table 3. AI Sphere Data Showing Total, Airmotor (No Sphere), and Sphere Deflections (D= 70 mm)

It is noted that deflections of 65 m/s projectiles at D = 38 mm are less than those for 40 m/s. This difference is explained by subsequent projectile analysis. Where total ΔL_L values are positive, the Air Motor contribution exceeds that of the sphere. Some general properties of dipoles are important in interpreting the above results. For a sphere, positioned with the projectile path in its equatorial plane, all field lines are normal to the projectile path. Their intensity is 1/2 the maximum dipole intensity and decreases as the inverse cube of the distance in the equatorial plane from the origin. The field intensity along the vertical axis also decreases as the inverse cube distance from the origin. The field intensity of the airmotor dipole on the sphere dipole equatorial plane is clearly more complicated.

D. Sphere and Airmotor Dipole Fields

Figure 3 presents schematics of Ω dipole fields for rotating spheres and airmotor rotor fields. Figure 3A is schematic of the Ω field dipole due to a right (CCW) rotating sphere not including the driving airmotor field. In Figure 3A, the projectile crosses the sphere in its equatorial plane and in front of it. The field lines are everywhere normal and downward (negative) to the equatorial plane. In 3B, the airmotor rotor dipole appears without the attached sphere. The location of the detached sphere (dashed) is indicated schematically along with the projectile path location. The distance between the sphere and airmotor centers is about 130 mm. Only those field lines emanating from the top of the rotor dipole which have a vertical component normal to the 3A sphere's equatorial plane interact with the projectile. These lines occupy a space plus and minus about 45 degrees from the axis at the center of the armature dipole. All of the rotor field lines with a vertical component are positive and diminish the sphere's negative field direction along the projectile path in the equatorial plane.

Thus, depending on the rotor field strength, the resulting projectile acceleration vector $\Omega \times \mathbf{V}$ can be either positive or negative. For solid spheres, the $\Delta \mathbf{L}_R$ field strength along the projectile path exceeds that of the airmotor dipole and yields a positive deflection of the projectile due to the spheres dipole field. Similar results were obtained for left rotations except not all deflections are negative indicating that in some cases the airmotor contribution exceeds that of the solid sphere or creates a more complex field.

Figures 3C and 3D are the corresponding dipoles for clockwise (left) rotations. Figure 3C shows the Ω field dipole due to a clockwise rotating sphere not including the driving airmotor field. In Figure 3C, the projectile again crosses the sphere in its equatorial plane and in front of it. The field lines originate at the bottom of the rotating sphere and are everywhere normal to the equatorial plane pointing upward (positive). The resulting $\Omega \times \mathbf{V}$ projectile acceleration is negative. In 3D, the airmotor rotor dipole appears without the attached sphere. The location of the detached sphere (dashed) is indicated schematically along with the projectile path location. Field lines emanating from the bottom of the rotor dipole cross the 3C equatorial plane from above, but only field lines having a vertical component at the 3C sphere's equatorial plane contribute to the $\Omega \times \mathbf{V}$ projectile acceleration. These lines occupy a space plus and minus about 45 degrees from the axis at the center of the 3C dipole. All of the rotor field lines with a vertical component crossing the 3C equatorial plane are negative and diminish the sphere's positive field strength along the projectile path. The positive Total $\Delta \mathbf{L}_L$ deflections in Tables 1 and 2 show that the airmotor contribution for two cases exceeds that of the solid sphere. These are for the 65 m/s projectile and for the 40 m/s projectile for the D = 70 mm location.

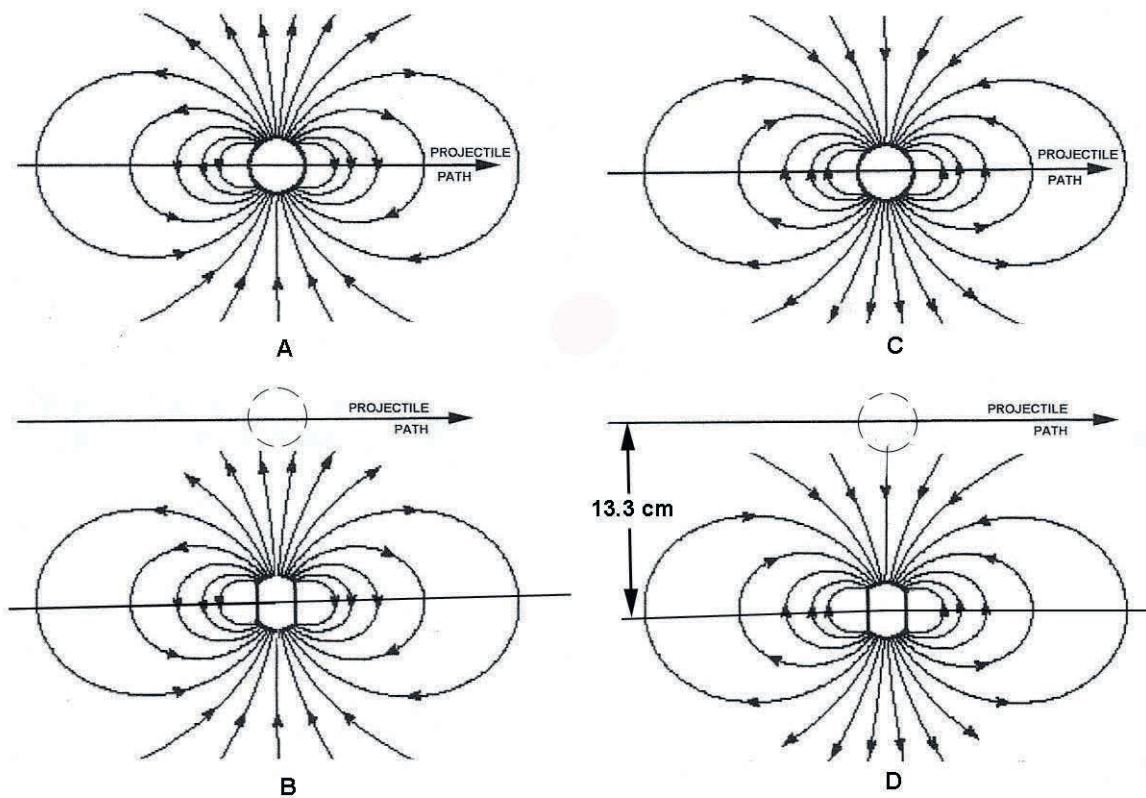


Figure 3. Generic dipole diagrams of right and left rotating spheres and airmotor rotors. Viewed from the side, 3A and 3B represent right rotations; 3C and 3D left rotations.

E. Co-Field Theory Predicted Deflections and Resolution with Experimental Data

Starting with the equation for inertial dipole as presented in Equation 19,

$$\Omega = \frac{\mu_{0g}\mu_g}{4\pi R^3} \quad (19)$$

The solid sphere is chosen as the baseline where μ_{0g} is defined in Equation 13. For μ_g , the inertial moment equals $(M/T) A$ where M is a mass in circular orbit with period T and area A . This can be defined as $I\omega_0/2$ where I is the moment of Inertia and ω_0 is the angular velocity.

$$\mu_g = k \frac{mR_0^2 \omega_0}{2} \quad (39)$$

In Equation (39), for a solid sphere, $m = M$, $K = 0.4$. For the hollow sphere with wall thickness of 0.138 mm, $k = 0.59$, $m = 0.33M$.

$$\mu_{0g}\mu_g = 4\pi k \frac{m}{M} R_0^3 \omega_0 \quad (40)$$

The co-field along the axis of the dipole is, with $\Omega_0 = 2\omega_0$,

$$\Omega = \frac{k m}{2 M} \left[\frac{R_0^3}{R^3} \right] \Omega_0 \quad (41)$$

The co-field in the equatorial plane of the dipole, and normal to it, is half that along the axis

$$\Omega = \frac{k m}{4 M} \left[\frac{R_0^3}{R^3} \right] \Omega_0 \quad (42)$$

where R_0 is the radius of the spinning sphere, and k is a constant which defines its moment of inertia, $I = k m R_0^2$. For spheres such as used in this experiment, $K = 0.4$. D is the sphere offset from the projectile path. The angular velocity of the sphere is ω . From Figure 1, the acceleration resulting from an object moving in the equatorial plane with velocity V is

$$\mathbf{a} = \boldsymbol{\Omega} \times \mathbf{V} \quad (43)$$

Since Ω is normal to and V is in the sphere's equatorial plane, the deflecting acceleration, \mathbf{a} , is normal to \mathbf{V} and in the equatorial plane.

$$\mathbf{a} = \frac{k m}{4 M} R_0^3 \Omega_0 \left[\frac{V}{(D^2 + L^2)^{3/2}} \right] \quad (44)$$

$$\mathbf{a} = A \frac{V}{(D^2 + L^2)^{3/2}} \quad (45)$$

$$\Delta V = \int \mathbf{a} dt \quad (46)$$

Noting that $L = Vt$, and $dt = dL/V$, Equation (46) becomes

$$\Delta V = \int \frac{AdL}{(D^2 + L^2)^{3/2}} \quad (47)$$

$$\Delta V = \frac{A}{D^2} \frac{L}{(D^2 + L^2)^{1/2}} \quad (48)$$

$$\Delta L = \int \frac{A}{VD^2} \frac{LdL}{(D^2 + L^2)^{1/2}} \quad (49)$$

$$\Delta L = \frac{A}{VD^2} (D^2 + L^2)^{1/2} \quad (50)$$

$$\Delta L = \frac{k}{4VD^2} \frac{m}{M} R_0^3 \Omega_0 (D^2 + L^2)^{1/2} \quad (51)$$

$$\Delta L_{\text{(Sphere)}} = \left[\frac{k}{4VD^2} \frac{m}{M} R_0^3 \Omega_0 (D^2 + L^2)^{1/2} \right]_{-L_1}^{L_2} \quad (52)$$

Equation (52) applies to both right and left rotations of the sphere. The deflections should be equal in magnitude for the same displacement, projectile velocity, and sphere angular velocity, but the left rotation deflections should be negative. Table 4 lists inputs for Equation (52).

SOLID SPHERE INPUTS FOR EQUATION (52)							
D	V m/s	k	Mass	R ₀ m	Ω ₀ Rad/s	L ₁ m	L ₂ m
38 mm	40	0.4	M	2.54E-02	3352	6.70E-02	0.883
38 mm	65	0.4	M	2.54E-02	3352	6.70E-02	0.883
70 mm	40	0.4	M	2.54E-02	3352	6.70E-02	0.883

Table 4. Data for Evaluating Equation (52)

Table 5 compares the ΔL_R and ΔL_L experimental results with calculations from Equation (52). Quantities with R subscripts refer to a right rotating solid sphere; L subscripts to a left rotating solid sphere.

V= 40 m/s D1=38mm	Measured	Measured	Calculated	Multiplier	Multiplier
Deflections	ΔL _R (mm)	ΔL _L (mm)	ΔL (mm)	K _R	K _L
Total	2.11	-0.52			
Air-Motor	1.04	1.8			
Sphere	1.07	-2.32	77	0.014	0.030
V= 65 m/s D1=38mm	Measured	Measured	Calculated	Multiplier	Multiplier
Deflections	ΔL _R (mm)	ΔL _L (mm)	ΔL (mm)	K _R	K _L
Total	2.43	1.05			
Air-Motor	1.89	1.42			
Sphere	0.54	-0.37	47	0.012	0.008
V= 40 m/s D2=70mm	Measured	Measured	Calculated	Multiplier	Multiplier
Deflections	ΔL _R (mm)	ΔL _L (mm)	ΔL (mm)	K _R	K _L
Total	2.58	0.65			
Air-Motor	0.58	0.85			
Sphere	2.00	-0.02	22	0.091	0.009

Table 5. Comparison of experimental data with Co-Field theory predictions

Equation (52) predicts that, for the solid sphere at the D = 38 mm location with 40 m/s projectiles, ΔL = 77 mm. For the 65 m/s projectile at the same D = 38 position ΔL = 47. For the solid sphere at the D = 70 mm location

with 40 m/s projectiles $\Delta L = 22$ mm. The respective measured deflections ΔL_R were 1.07, 0.54, and 2.00 mm. Equation (52) thus greatly over predicts ΔL_R projectile deflections at the $D = 38$ solid sphere location by factors of 77 and 47, and that at the $D = 70$ location by a factor of 22.

The large difference between experimental and calculated values requires a Co-Field Factor to bring the predicted values into agreement with experiment. Such calculated Co-Field Factors, K_R and K_L , corresponding to right and left rotations, appear in Table 5. The factor K_R for both 40 and 65 m/s for location $D = 38$ is similar. K_R for the $D = 70$ location is a factor of 7 larger due to the lower airmotor contribution. The Co-Field Factor, K , thus appears as a required multiplier of Co-Field theory predictions.

$$\Delta L_{Meas} = K \left[\frac{k}{4VD^2} \frac{m}{M} R_0^3 \Omega_0 (D^2 + L^2)^{1/2} \right]_{-L1}^{L2} = K \Delta L_{Calc} \quad (53)$$

The Co-Field Factor is presented as separate for each result in Table 5. Experiments not including an airmotor component might reveal it as a single fundamental constant.

A second, independent, data set exists which requires a Co-Field Factor. That data set is the collection of anomalous deflections of spacecraft flybys of the earth.

V. FLYBY ANOMALOUS DEFLECTIONS -- The Original Experimental Data

The first data supporting the author's Co-Field theory [1] was discovered in the the Anderson, et al. paper [2]. The semi-empirical interpretation of anomalous earth-spacecraft flyby deflections appeared similar to the predicted $2\boldsymbol{\omega} \times \mathbf{V}$ acceleration of an object moving in an inertial dipole field. In the flybys, the spacecraft followed a hyperbolic path essentially approaching and exiting the earth's gravitational influence along asymptotes connected with an arc having a distance H of closest approach. Anderson, et.al. [2] analyzed the anomalous flyby data and found that the velocity change for the spacecraft flybys of the earth can be described as

$$\Delta \mathbf{v}_\infty = 2\boldsymbol{\omega}_E \mathbf{v}_\infty (\cos \delta_i - \cos \delta_o) \frac{R_E}{c} \quad (54)$$

where $\Delta \mathbf{v}_\infty$ is the observed anomalous velocity deflection. $\boldsymbol{\omega}_E$ is the earth's angular velocity. \mathbf{v}_∞ is the spacecraft velocity along the incoming and outgoing asymptotic velocities. The $\mathbf{v}_\infty \cos \delta$ terms are the respective components of the spacecraft's asymptotic incoming and outgoing velocities normal to $\boldsymbol{\omega}_E$, the earth's angular velocity. The δ terms are the respective inertial declinations. Equation (54) in vector form becomes

$$\Delta \mathbf{V}_\infty = (2\boldsymbol{\omega}_E \times \mathbf{v}_{\infty i} - 2\boldsymbol{\omega}_E \times \mathbf{v}_{\infty o}) \frac{R_E}{c} \quad (55)$$

The $2\boldsymbol{\omega} \times \mathbf{v}$ terms are accelerations. $\Delta \mathbf{V}_\infty$ is a velocity normal to the outgoing asymptotic velocity and to the earth's angular velocity. R_E/c is the effective time interval during which the change in velocity occurs. This ratio of the earth radius to the speed of light is 0.0212 sec. The physical significance of the ratio is not obvious other than it is a time interval fit to the data. The path of the spacecraft flying by the earth is hyperbolic. The orbital path can be approximated by incoming and out-going straight line asymptotes connected by an arc whose apex is the point of closest approach, H . The deflection, $\Delta \mathbf{V}_\infty$, occurs during the transverse of the arc. The arc

resulting from the earth's gravity on the spacecraft connecting the asymptotes can be approximated by $R\theta$ where R is the sum of R_E , the earth's radius and H , the altitude of closest approach. The angle θ is the angle of transition between the asymptotes. The average velocity V in traversing $R\theta$ is between V_∞ and the velocity at closest approach, V_f . The average is assumed here. The data from the NEAR Flyby are used for this example, although essentially the same results would be obtained using averages of corresponding points from all flybys. Using the values from the NEAR Flyby, which yielded the largest anomalous deflection: $R_E = 6371$ km, $H = 539$ km, the average $R = 6910$ km, $\theta = 1.07$ radians, $V_\infty = 6.851$ km/s, $V_f = 12.739$ km/s, $V_{Ave} = 9.795$ km/s. Preserving the R_E/C time of 0.0212 sec, and noting that V is $\ll C$, a constant multiplier K_F is introduced.

$$R_E/C = K_F R\theta / V \quad (56)$$

Equation (56) provides a physical basis for the spacecraft deflection time. It yields $K_F = 0.028$; $R\theta / V = 0.755$ sec for the Flyby spacecraft. Restating equation (55), the physical description of the Flyby anomalous deflections becomes

$$\Delta V_\infty = K_F (2\omega_E \times v_{\infty i} - 2\omega_E \times v_{\infty o}) \frac{R\theta}{V} \quad (57)$$

This interpretation of the Flyby experiment R_E/C term defines a projectile path of the spacecraft in the transition region between the asymptotes. This is physically more plausible and makes the Flyby results fully compatible with the predictions of the Co-Field model. This includes the identification of a Co-Field Factor whose value, $K_F = 0.028$, is in the range of values found in the Co-Field experiments. The anomalous velocity change described in the semi-empirical Equations (53) and (54), and in Equation (56), occurs at the end of the arc transition acceleration and remains constant as it proceeds along the receding asymptote. The subsequent deflection is given by $\Delta L = \Delta V_\infty t$. A more detailed analysis of the Flyby Anomaly relative to the co-field model appears in a previous paper [6].

VI. SUPPLEMENTAL SPHERE-ONLY DEFLECTION EXPERIMENTS

The series of experiments reported above showed that a rotating sphere deflects a projectile moving in its equatorial plane. The rotation direction determines the deflection direction. In these co-field experiments, the sphere attached directly to the airmotor. The data revealed that the airmotor rotor provided a significant part of the measured deflection. Removal of the sphere permitted measurement of the airmotor induced deflection. Subtraction of the airmotor induced deflection from the total yielded the sphere-induced projectile displacement. A limited number of experiments were conducted with the sphere and airmotor at larger separation as a check on the results for the above sphere-only induced deflections.

The Co-Field theory [1], predicts that a rotating object creates a surrounding inertial dipole field that interacts with a projectile moving past it. Since a dipole field strength diminishes as the inverse cube distance from the source, separating the airmotor from the sphere should reduce the effect of the airmotor rotor dipole field on the total projectile deflection. Such a separation with a 6.35 mm diameter fiberglass connecting rod, positioned the airmotor further below the sphere. The resulting center-center sphere-airmotor rotor separation was 545 mm. The original separation was 130 mm. This separation reduces the rotor field at the sphere by a factor of about 100. Tests with the sphere removed revealed only small erratic projectile deflections identified as noise. In tests with spheres attached, the measured deflections are thus due to projectiles interacting with only the sphere field.

Table 6 summarizes the results from the original close-coupled geometry. In Table 6, the deflections attributed to the airmotor rotor are comparable or larger than those of the sphere. Table 7 summarizes data from the separated sphere-airmotor. In Table 7, the deflections are larger than comparable ones in Table 6. This is

partially due to the lower projectile velocities in the separated geometry. The remaining difference is likely due to the more complicated interaction of the airmotor field in the close coupled experiments of Table 6. The essential properties of the data are still positive for right rotations, negative for left rotations of the sphere. The deflections for left rotations are larger than those for right rotations in both cases. The supplemental experiment thus supports the data analysis of the previous experiments and provides a more direct set of measurements.

Close-Coupled Sphere-Airmotor				
Expt. Geometry	Deflections		Projectile Velocity	
D=38 mm;	ΔL_R mm	ΔL_L mm	V_R m/s	V_L m/s
Sphere+Air Motor	2.11	-0.52	40	40
Air Motor	1.04	1.8	40	40
Sphere	1.07	-2.32		

Table 6. Close Coupled Solid Sphere-Airmotor Data Summary

Separated Sphere-Airmotor				
Expt. Geometry	Deflections		Projectile Velocity	
D=41 mm;	ΔL_R mm	ΔL_L mm	V_R m/s	V_L m/s
Sphere	2.61	-3.41	29	37

Table 7. Separated Solid Sphere-Airmotor Data Summary

Close Coupled/ Separated Spheres	Measured	Measured	Calculated	Multiplier	Multiplier
Deflection	ΔL_R (mm)	ΔL_L (mm)	ΔL (mm)	K_R	K_L
Close C'pled Sph: V= 40m/s ;D=38 mm	1.07	-2.32	77	0.014	0.030
Separated Sph: V_R = 29 m/s ; D=41 mm	2.61		91	0.029	
Separated Sph: V_L= 37 m/s ; D=41 mm		-3.41	71		0.048

Table 8. Experimental Deflections, Calculated Deflections, and Required Co-Field Factors

Table 8 compares the measured values of the close coupled and separated sphere-airmotor deflections and their calculated values. As in Table 5, the calculated values are again much larger than the measured deflections. Thus, the calculated deflection values for all the co-field experiments require a Co-Field multiplier to agree with experiment. For the 50.8 mm solid spheres of Table 8, with a range of, displacements, separations and projectile velocities, the Co-Field factors ranged from 0.014 to 0.048. The comparable K value, K_F , for the flyby experiments was 0.028.

Table 9 averages the ΔL_R and ΔL_L values from the co-field experiments to obtain single average K values. Averaging the two values may actually be a better measure of the deflections than treating them separately. That they are different suggests that the left rotation result is asymmetric due to the airmotor connection.

Close Coupled/Separated/Flyby	Measured	Calculated	Calculated		
Deflection Source	ΔL_{ave}	ΔL (mm)	K_{ave}	V_{ave}	D
Close Coupled Sphere	1.7 mm	77	0.022	40 m/s	38 mm
Separated Sphere-Airmotor	3.01mm	80	0.038	33 m/s	41mm
Flyby Deflection	13.46 mm/s	-	0.028	9.8 km/s	539 km

Table 9. K values from averages of ΔL_R and ΔL_L Co-Field deflections compared to Flyby data.

In Table 9, The K values are remarkably similar despite differences in average projectile velocities and distances, D, of closest approach. The average of the three K values is 0.028. These results suggest that a

universal Co-Field K constant might exist to bring calculated co-field projectile deflections into agreement with experimental data.

VII. SUMMARY AND CONCLUSIONS

Projectiles fired past rotating solid and hollow aluminum spheres, along their equatorial planes, produced projectile deflections. The majority of the experiments had the sphere attached directly to the airmotor. The deflections from these experiments included contributions from the rotor of the airmotor driving the rotation. To get the deflections due to the spheres alone, it was necessary to subtract the rotor contributions. To support the validity of this analysis, limited auxiliary experiments separated the sphere and airmotor rotors by 545 mm. This eliminated airmotor contributions from the total deflections resulting in "sphere-only" deflections. A third data set, the spacecraft Flyby data, was analyzed in the context of the Co-Field model. A summary of experimental results includes:

Sphere-Only Deflections: (A) The projectile deflections for right (counterclockwise) sphere rotation ΔL_R were positive; those for Left (clockwise) rotation, ΔL_L , negative, as required by the Co-Field theory. (B) The most definitive data were for solid spheres and 40 m/s projectile velocities. This configuration was chosen as the reference. (C) Right and left deflections were not equal as predicted by the theory, probably due to asymmetries at the poles. (D) The results of the separated sphere-airmotor experiments supported the close coupled results but with larger deflections. Differences are due, at least in part, to lower projectile velocity and larger distance of closest approach. (E) Separation of the sphere and airmotor, as predicted by the Co-Field dipole model, effectively removed the airmotor rotor contribution consistent with the inverse cube prediction of field intensity with distance from its source.

Co-Field Factors:

Deflection values for ΔL_R and ΔL_L were in the range of a few millimeters. The calculated value was 77 mm for the base case and 91 and 71 mm, respectively, for ΔL_R and ΔL_L for the separated sphere-airmotor case. Averaging ΔL_R and ΔL_L values yields K values of 0.022 and 0.038 for the close coupled and separated sphere geometries, respectively. The Co-Field Factor for the Flyby experiments is $K_F = 0.028$. The closeness of the K factors for a wide range of conditions suggests a universal K factor.

Correlation of Experiment and Co-Field Theory

The Co-Field theory predicts an angular velocity dipole gravitational co-field surrounding a spinning body and the deflection of a projectile moving in that field. The following experimental results support the Co-Field model:

- Measured right or left deflections depending on rotation direction of the sphere.
- Larger deflections for more massive, solid spheres than for hollow spheres.
- Field intensity decreases with distance from the source as shown by separation of the sphere and airmotor thus eliminating the airmotor rotor-sphere interaction.
- For the geometry of the present experiments, higher projectile velocities produced smaller deflections.
- The spacecraft flyby data and its semi-empirical description are consistent with the Co-Field model. A re-interpretation of its deflection time yields a similar K factor multiplier as the present experiments.
- The deflection predictions of the Co-Field model for the present experiments and the Flyby data K_F factor yield an average K factor multiplier of 0.029.

In conclusion: This experimental study provided verification for the gravitational Co-Field of a spinning object and for the theory predicting its interaction with a moving projectile. It provided an explanation for the Flyby Anomaly. It revealed a requirement and range for a Gravitational Co-Field Factor. The Gravity and Co-Field theory combination also provides a method for describing gravitational waves in a classical format. More speculatively, it may result in the development of Gravitational & Co-Field machines analogous to those of Electricity and Magnetism, perhaps on a nano scale.

Acknowledgement

Reviews of the manuscript and useful discussions with Jerry F. Cuderman II are gratefully acknowledged.

REFERENCES

- [1] J.F. Cuderman, "A theory of the gravitational co-field and its application to the spacecraft flyby anomaly" viXra:1610.0299 v1 (2016)
- [2] John D. Anderson, James K. Campbell, John E. Ekelund, Jordan Ellis, and James F. Jordan, "Anomalous orbital-energy changes observed during spacecraft Flybys of earth," Phys. Rev. Lett. **100**, 091102 (2008).
- [3] Slava G. Turyshev and Viktor T. Toth, "The puzzle of the flyby anomaly," Space Science Rev. **148**, 168-174 (2010).
- [4] H.Helmholtz, "Ober integrate der hydrodynamischen Gleichungen, welcher der Wirbelbewegungen entsprechen" Journal fur die reine und angewandte Mathematik **55**, 25-55 (1858)
- [5] O. Heaviside, in "A Gravitational and Electromagnetic Analogy," The Electrician (The Electrician printing and publishing company, London, 1893) Chap. 31, pp. 281-282.
- [6] J.F. Cuderman, "Explanation of the spacecraft flyby anomaly" viXra:1707.0324 v1 (2017)